Role of lattice distortion and A site cation in the phase transitions of methylammonium lead halide perovskites

Jonathon R. Harwell,[1] Julia L. Payne,[2] Muhammad T. Sajjad,[1] Frank J. L. Heutz,[2] Daniel M. Dawson,[2] Pamela S. Whitfield,[3,*] John T. S. Irvine,[2] Ifor D. W. Samuel,[1] and Michael A. Carpenter[4]

[1]*Organic Semiconductor Centre, Scottish Universities Physics Alliance, School of Physics and Astronomy, University of St Andrews, North Haugh, St Andrews, KY16 8HA, Fife, United Kingdom*

[2]*EaSTChem, School of Chemistry, University of St Andrews, North Haugh, St Andrews, KY16 9ST, Fife, United Kingdom*

[3]*Chemical and Engineering Materials Division, Neutron Sciences Directorate, Oak Ridge National Laboratory, Oak Ridge, Tennessee 37831, USA*

[4]*Department of Earth Sciences, University of Cambridge, Downing Street, Cambridge CB2 3EQ, Cambridgeshire, United Kingdom*

(Received 2 February 2018; published 20 June 2018)

The rapid increase in power conversion efficiencies of photovoltaic devices incorporating lead halide perovskites has resulted in intense interest in the cause of their excellent properties. In the present paper, resonant ultrasound spectroscopy has been used to determine the elastic and anelastic properties of $CH_3NH_3PbX_3$ (where X = Cl, Br, or I) and $CD_3ND_3PbI_3$ perovskites in the 5–380 K temperature range. This is coupled with differential scanning calorimetry, variable temperature neutron powder diffraction, and variable temperature photoluminescence studies to provide insights into the underlying processes and structural instabilities in the crystal structure. By comparing measurements on $CH_3NH_3PbI_3$ with the deuterated equivalent, it has been possible to distinguish processes which are related to the hydrogen bonding between the methylammonium cation and the perovskite framework. We observe that replacing hydrogen with deuterium has a significant impact on both the elastic and photophysical properties, which shows that hydrogen bonding plays a crucial role in the material performance. Temperature-dependent photoluminescence studies show that the light emission is unaffected by the tetragonal-orthorhombic phase transition, but a blueshift in the emission and a steep increase in photoluminescence quantum yield are seen at temperatures below 150 K. Finally, observations of peaks in acoustic loss occurring in $CH_3NH_3PbCl_3$ have revealed freezing processes in the vicinity of $\sim$150−170 K, with activation energies in the range of 300 to 650 meV. These processes are attributed to freezing of the motion of methylammonium cations, and could explain the changes in photoluminescence seen in $CH_3NH_3PbI_3$ at the same temperature.

DOI: 10.1103/PhysRevMaterials.2.065404

I. INTRODUCTION

Since their first demonstration as a solar cell material in 2009 [1], organolead halide perovskites have proven to be a stimulating discovery relevant to a wide range of research fields. Their hybrid nature, mixing the properties of both organic and inorganic semiconductors, has earned them significant attention as materials for solution processed solar cells [2], light emitting diodes [3], lasers [4], and thermoelectric devices [5]. These hybrid perovskites are now rapidly becoming competitive with the more established materials in their respective fields, but the precise reasons for their high performance remain poorly understood. In particular, methylammonium lead iodide ($CH_3NH_3PbI_3$) and its variants have been studied using a variety of techniques in order to gain an insight into the origins of their properties [6–9]. A good understanding of the structure-property relationships in organolead halides could lead to the design of new materials with even higher performance and may even allow the replacement of their toxic lead component [10].

The electrical [11], thermal [12], and photophysical [13] properties of the $CH_3NH_3PbX_3$ (X = Cl, Br, or I) phases have been investigated in detail. Studies of phase transitions in classical oxide perovskites and in metal organic frameworks with the perovskite structure have shown that coupling of the order parameter with strain has a strong influence both on the intrinsic structure-property relationships and on the nature and dynamics of transformation microstructures [14]. The most sensitive measure of such coupling is provided by variations in elastic and anelastic properties, but these have so far not been determined for the methylammonium lead halide compounds. In the present paper, resonant ultrasound spectroscopy (RUS) is used in combination with neutron-diffraction and photoluminescence (PL) data to focus on strain-related aspects of instabilities in the $CH_3NH_3PbX_3$ structure and to investigate their potential impact on other material properties. RUS is an advanced technique for measuring the elastic constants and acoustic loss in a material [15]. It is already used extensively in the study of inorganic oxide perovskites [14] and has played a key role in the study of new piezoelectric materials [16], superconductors [17], and ferroelectrics [18]. Here changes in

*Present address: Excelsus Structural Solutions (Swiss) AG, Park innovAARE, 5234 Villigen, Switzerland.

elastic properties are also correlated with changes in lattice parameters and PL.

Perovskites have the general formula ABX_3, where A and B are cations and X is the anion. The simple, cubic perovskite adopts space group $Pm\bar{3}m$ and consists of corner-sharing B-centred BX_6 octahedra, with the A cation located in the center of the cavity formed by the corner sharing octahedra. The Goldschmidt factor, based on ionic radii, has been used for years to predict the stability region of the perovskite structure in oxide perovskites. Recent work by Travis *et al.* [19]. has shown that application of the tolerance factor incorrectly predicts the structure type adopted in the case of many inorganic halide perovskites. By using revised ionic radii which take covalency into account, revised stability fields for the halide perovskites may be formed. It is therefore also of interest to compare the behavior of organolead halide perovskites with that of oxide perovskites.

The structure of $CH_3NH_3PbI_3$ has been explored by a number of groups and $CH_3NH_3PbI_3$ has been found to have orthorhombic, tetragonal, and cubic polymorphs [20,21]. The structural models determined by Whitfield *et al.* [20] and Weller *et al.* [21] are shown in Fig. 1 and clearly depict the crystallographic disorder of the methylammonium cation. The difficulty in obtaining accurate structural models for $CH_3NH_3PbI_3$ is due to the dynamic disorder of the methylammonium cation around the ideal A site, X-ray scattering being dominated by the lead iodide framework and the large incoherent neutron-scattering cross section of hydrogen, which is particularly detrimental in powder neutron-diffraction studies. As a result, deuterated samples are required for high-quality neutron-diffraction studies. A further advantage of deuterated samples is that the additional mass from the deuterium atom causes significant differences in the hydrogen bonding of the $CD_3ND_3^+$ cation compared to $CH_3NH_3^+$, without a significant effect on the ionic radius. Due to coupling between the order parameters, the change in hydrogen bonding will also impact the tilting in some way. But this effect on the tilting is expected to be very small in comparison to the primary impact of the change in hydrogen bonding. The influence of the methylammonium cation on the properties of $CH_3NH_3PbX_3$ is a subject of intense interest [22,23], largely due to the strong hydrogen bonding it introduces, and hence in this paper we perform a direct comparison between $CH_3NH_3PbI_3$ and $CD_3ND_3PbI_3$. This allows us to observe changes which are dominated by the hydrogen bonding with minimal impact from other parameters, thus providing a powerful measure of the impact on the material properties.

The aim of this paper is to probe the elastic and anelastic properties of $CH_3NH_3PbX_3$ (X = Cl, Br, or I) and $CD_3ND_3PbI_3$ over a wide temperature range using resonant ultrasound spectroscopy to understand how the underlying strains, disorder, and hydrogen bonding impact the properties of the material. The impact of the hydrogen bonding in particular has been a subject of intense recent interest, and we distinguish the effects of this process by performing parallel studies on both deuterated and nondeuterated versions of $CH_3NH_3PbI_3$. This comparison shows differences which are dominated by the change in hydrogen bonding, allowing us to determine which processes are directly impacted by this effect.

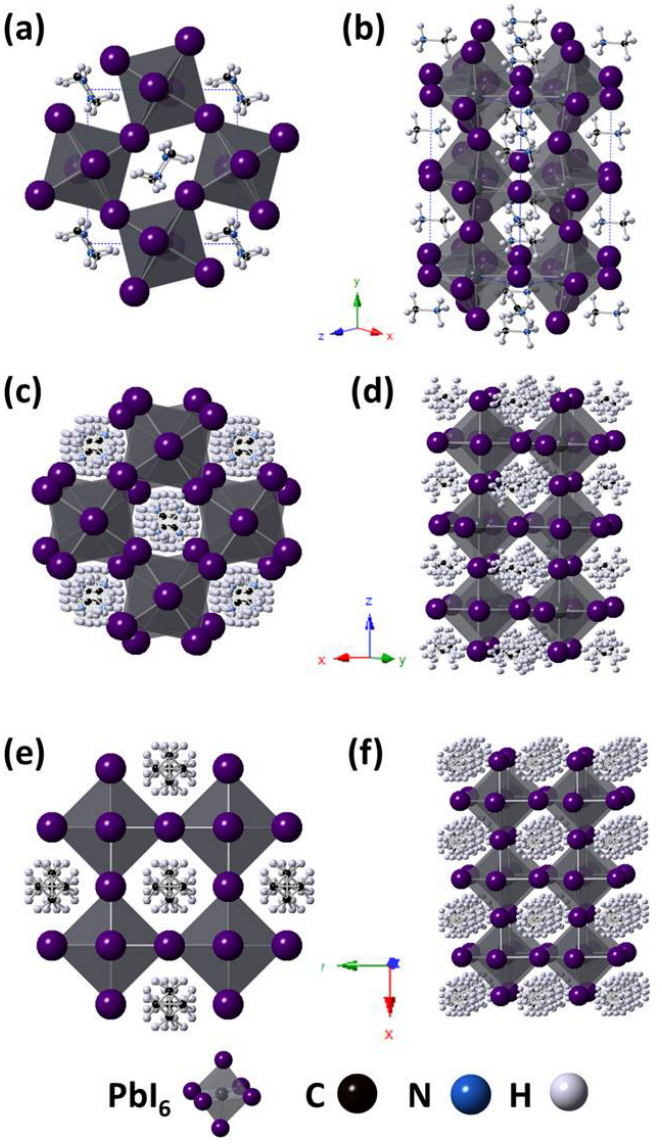

FIG. 1. Structures adopted by $CH_3NH_3PbI_3$ as determined by Whitfield *et al.* [20]. (a, b) Orthorhombic, *Pnma*. (c, d) Tetragonal, $I4/mcm$. (e, f) Cubic, $Pm\bar{3}m$. (a) *ac* plane. (c) *ab* plane.

II. EXPERIMENTAL

A. Synthesis and characterization of $CH_3NH_3PbX_3$ (X = Cl, Br, or I) and $CD_3ND_3PbI_3$

1. Synthesis of $CH_3NH_3PbX_3$ *(*X = Cl, Br, *or* I*)*

We added 2 ml of concentrated HX (X = Cl, Br, or I) to CH_3NH_2 (33%, EtOH) at 0 °C (using an ice bath) under constant stirring. Lead acetate trihydrate was dissolved in HX at 100 °C. The lead-containing solution was added dropwise to the methylammonium halide solution. The samples were left on a hotplate overnight at 75 °C. White, orange, and black crystals formed, depending on the halide (Cl, Br, or I, respectively). The resulting crystals were filtered, washed with toluene, and dried. $CH_3NH_3PbI_3$ was filtered while hot to avoid formation of the hydrated phase while in contact with the mother liquor.

2. *Synthesis of* $CD_3ND_3PbI_3$

The synthesis of $CD_3ND_3PbI_3$ was carried out under an argon atmosphere using standard Schlenk techniques. All glassware was dried prior to use to remove traces of water. To begin with, an aqueous solution of CD_3ND_2 was made by condensing CD_3ND_2 gas into a solution, using a dry ice acetone bath and an acetone-dry ice condenser. D_2O was added to the CD_3ND_2 (l) to make a 43.7% solution. DI was added to lead acetate trihydrate and the mixture was stirred at 95 °C, until the lead salt had completely dissolved. The CD_3ND_2 solution was cooled to 0 °C (using an ice-water bath) and DI was added to this solution, dropwise, while stirring continually. All solutions were transferred using a syringe to minimize air exposure. The Pb-containing solution was added dropwise to the CD_3ND_3I solution. The resulting solution was heated to 95 °C for 3 h and then left at 75 °C overnight, under argon. The DI solution was removed by syringe and the sample filtered, washed with toluene, and dried.

B. Characterization

1. *Powder neutron diffraction*

Prior to powder neutron-diffraction studies, crystals of $CD_3ND_3PbI_3$ (from the same batch as used in the RUS study) were ground into a powder. Variable temperature time-of-flight powder neutron-diffraction data were collected for $CD_3ND_3PbI_3$ using a Janis Cryofurnace on the POWGEN beamline, at the Spallation Neutron Source, Oak Ridge National Laboratory, Tennessee, USA. Data were collected using a 1-Å band centered about 2.665 Å. Lattice parameters were obtained from sequential Rietveld refinement using GSAS/EXPGUI [24,25]. The structural model previously reported by Whitfield *et al.* was used as the starting model for Rietveld refinement [20].

2. *Differential scanning calorimetry*

Differential scanning calorimetry data were collected using a Netzsch 204 F1 Phoenix DSC. The sample was cooled and heated between 373 and 113 K at a rate of 5 K min^{-1}.

3. *NMR*

Solid state NMR was used to probe the level of deuteration in the $CD_3ND_3PbI_3$ sample. Solid-state ^1H NMR spectra were obtained using a Bruker Avance III spectrometer, equipped with a 9.4-T wide-bore superconducting magnet (^1H Larmor frequency of 400.13 MHz). Samples were packed into conventional 1.9-mm ZrO_2 rotors and rotated at a MAS rate of 30 kHz. Spectra were acquired with a rotor-synchronized spin-echo pulse sequence with echo delay of 33.3 μs in order to remove the large probe background signal. Pulses were applied with a nutation frequency ($\omega_1/2\pi$) of ~100 kHz with signal averaging carried out for 16 transients with a repeat interval of 60 s. Spectra were referenced to $(CH_3)_4Si$ using the NH_3 resonance of solid L-alanine ($\delta = 8.5$ ppm) as a secondary reference. Solid state NMR spectra showed a small percentage of H on the ND_3 group of $CD_3ND_3PbI_3$.

C. Time resolved photoluminescence setup

To measure the time resolved photoluminescence of a sample, crystals were crushed into a powder and placed between two 10-mm quartz disks to hold the powder in place. These disks were transferred to a specialized holder which was then placed in an Oxford Instruments nitrogen cryostat, with transparent windows to allow optical measurements on the sample, and pumped down to a pressure lower than 10^{-4}mbar. The sample temperature was controlled using liquid nitrogen and an ohmic heater in a cold finger setup, so that set points between 77 and 300 K could be obtained. To measure photoluminescence, the sample was optically excited with 515-nm light from a Light Conversion regeneratively amplified Pharos Laser with 200-fs pulses. The remaining pump light was then filtered out and the photoluminescence was measured with a Hamamatsu streak camera.

D. Resonant ultrasound spectroscopy setup

The RUS setup used for measurements below room temperature consists of a home built transducer head controlled by Dynamic Resonance System (DRS) Modulus II electronics, as described by McKnight *et al.* [26]. A single crystal is placed between two piezoelectric transducers, with one acting as a resonator and the other as a sensor. The RUS head is attached to the end of a stick and lowered into an Orange 50-mm helium flow cryostat, supplied by AS Scientific Products, Ltd. Temperature regulation and measurement are achieved using a silicon diode and a LakeShore model 340 controller, and the overall precision for the sample temperature is in the range of ± 0.1 K.

The setup used for RUS measurements above room temperature has alumina rods protruding horizontally into a Netzsch 1600 °C furnace. The sample is placed between the ends of the rods inside the furnace, with piezoelectric transducers attached to the other end of each rod, as described in detail by McKnight *et al.* [27]. It is still possible to collect good quality spectra, but they also contain peaks due to resonances of the buffer rods. Temperature is recorded with a thermocouple sitting a few millimeters away from the sample. A small correction is usually made to this temperature, as calibrated from measuring the transition point (846 K) of a quartz standard, to give an estimated accuracy of ± 1 K.

E. Data collection and analysis

Single crystals used for RUS measurements were checked optically for the absence of cracks and then selected on the basis of which ones gave the best quality spectra. All the chosen crystals were irregular in shape, with dimensions ~1×1×1 mm^3 and masses between 1 and 4 mg. At the start of each low-temperature experiment the sample chamber was evacuated and then filled with a few millibars of helium to act as exchange gas. Spectra containing 65 000 data points in the range 0.1–1.2 MHz were collected in automatic sequences of 5-K steps from ~295 to ~10 K and back again to room temperature. Some temperature intervals were covered in 1-K steps. A period of 20 min was allowed for thermal equilibration at each set point before data collection. The high-temperature

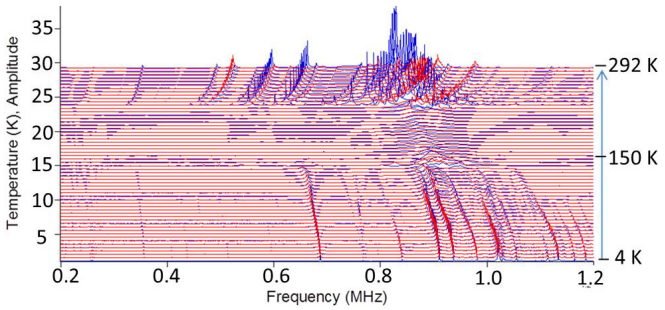

FIG. 2. Primary RUS spectra from a single crystal of $CH_3NH_3PbBr_3$. The spectra have been offset up the y axis in proportion to the temperature at which they were collected, such that the uppermost spectrum was collected at ~300 K, and the lowermost one was collected at ~5 K. Individual spectra were collected in 5-K intervals during cooling (blue lines) and heating (red lines).

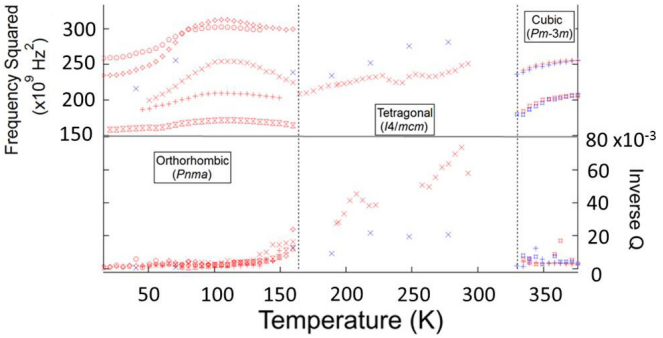

FIG. 3. Variation of f^2 (representing elastic constants) and Q^{-1} (representing acoustic loss) as a function of temperature, for different resonance peaks in a single crystal of $CH_3NH_3PbI_3$, scaled to be closer together for clarity. The phase transitions are shown by dotted lines. Blue and red points represent data collected on cooling and heating, respectively.

measurements were undertaken, also in automated sequences, with the sample sitting in air.

All spectra were analyzed using the software package Igor Pro 7.0 (Wavemetrics). For each sample, the spectra from the variable temperature data sets were first examined together and plotted with a y-axis offset proportional to the temperature at which they were collected. An example spectrum of $CH_3NH_3PbBr_3$ is shown on Fig. 2. Selected resonance peaks were fit using an asymmetric Lorentzian function to determine peak frequency, f, and width at half height, Δf, according to a standard procedure described by McKnight *et al.* [26,27]. Natural acoustic resonances of a small object are dominated by shearing motions and the related combination of single-crystal elastic constants for each resonance scale with f^2. An increase or decrease in the value of f^2 thus corresponds to elastic stiffening or softening of the shear elastic constants. The inverse mechanical quality factor, taken as $Q^{-1} = \Delta f/f$, is a measure of acoustic attenuation. It follows that graphs of f^2 and Q^{-1} versus temperature, plotted for each peak which can be followed in the spectra, show variations of the elastic constants and acoustic loss. The fitting process has uncertainties which are generally smaller than the symbols used to display values of f^2 and Q^{-1} in the graphs below. Real experimental uncertainties in the absolute values are hard to define but, in general, are suggested by the level of noise in the data. Significance is attached to the variations in f^2 and Q^{-1} only when they are greater than this level of background noise.

III. RESULTS

A. Methylammonium lead iodide, $CH_3NH_3PbI_3$

The complete sets of RUS spectra for $CH_3NH_3PbI_3$ are shown in the Supplemental Material (Figs. S1 and S2) [28]. Figure 3 shows the variations of f^2 and Q^{-1} with temperature obtained by fitting selected resonance peaks in them, collected on both the high- and low-temperature instruments. Values of f^2 have been rescaled arbitrarily so that the results from all the peaks can be compared on a single graph (Fig. 3). The sequence of transitions expected on the basis of several literature reports [20,21,29] is $Pm\bar{3}m$-$I4/mcm$-$Pnma$, with the cubic-tetragonal transition occurring at ~327 K and the tetragonal-orthorhombic transition at ~165 K. There has historically been some controversy on whether the space group of the tetragonal phase is polar [30] or nonpolar [20,29]. This is of direct interest for solar cells because a polar space group would be ferroelectric, and could explain the origin of the efficiency hysteresis observed in early iterations of perovskite solar cells. However, ferroelectricity has recently been shown by Alvar *et al.* [31] to be completely absent in $CH_3NH_3PbI_3$, which strongly supports the prevailing consensus that the space group is nonpolar.

Figure 3, along with the combined data from Figs. S1 and S2 in the Supplemental Material [28], show that there are three distinct temperatures in our RUS data (Figs. S1 and S2) corresponding to the known stability fields of the orthorhombic, tetragonal, and cubic structures [20,21,29,32]. DSC data in Fig. S3 in the Supplemental Material [28] show two anomalies on both heating and cooling, at 328 and 326 K and at 160 and 153 K, consistent with the reported results for tetragonal-cubic and orthorhombic-tetragonal transition temperatures.

Many peaks are visible in the RUS spectra at low (5–162 K) and high temperatures (>328 K), but they almost all disappear in the temperature interval corresponding to the stability field of the tetragonal structure. The few peaks which remain visible exhibit very high Q^{-1} values in comparison with the values for the cubic and orthorhombic phases. This further emphasizes the strong attenuation in the tetragonal phase. The Q^{-1} values for the orthorhombic structure increase slightly as the orthorhombic-tetragonal transition is approached from below, but there seems to be no equivalent precursor effect as the tetragonal-cubic transition is approached from above. From the abrupt changes in spectra at both transitions, the two transition temperatures have been taken to be $162 +/- 3$ and $328 +/- 3$ K. This is in good agreement with the DSC results, which show peaks for the orthorhombic to tetragonal transition at 159 K and 153 K on heating and cooling cycles respectively, with peaks for the tetragonal to cubic transition appearing at 328 K on heating and 326 K on cooling.

The second point to note from Fig. 3 is that the position of the individual resonances varies with temperature, when the jumps in peaks through phase transitions are ignored. While

it has not been possible to follow the evolution of all the resonances across the stability field of the tetragonal structure, the lowest-frequency modes clearly show the patterns of overall softening (falling values of f^2) and stiffening (increasing f^2). As the sample is cooled from 380 K towards the cubic to tetragonal phase transition, all resonance peaks indicate softening of the related elastic constants as the transition is approached. Peaks that are visible in spectra collected between ∼300 and ∼165 K also indicate slow softening with decreasing temperature for the tetragonal structure. Below the tetragonal-orthorhombic transition, all the resonances first indicate stiffening with falling temperature. However, at around 110 K this trend starts to reverse and the peaks all indicate rapid softening with further cooling. There is no concomitant increase in loss associated with this softening, showing that it is intrinsic and not caused by any anelastic defects in the material. The magnitude of the hardening and softening varies depending on which resonance peak is studied, reaching a total softening of ∼20% in the most affected peaks, but the overarching trend is the same regardless of the peak studied.

B. Methylammonium lead bromide, $CH_3NH_3PbBr_3$

$CH_3NH_3PbBr_3$ has a different expected phase evolution from the iodide with an additional phase between $I4/mcm$ and *Pnma* that has been suggested to be incommensurate [30]. Anticipated transition temperatures for the sequence $Pm\bar{3}m$ (cubic)-$I4/mcm$ (tetragonal)-incommensurate-*Pnma* (orthorhombic) are ∼235,∼154, and ∼148 K [33]. Figure 2 shows the variable temperature RUS spectra collected on a single crystal of $CH_3NH_3PbBr_3$ between 5 and 300 K in 5-K intervals. Like $CH_3NH_3PbI_3$, the resonance peaks are barely visible in the stability field of tetragonal $CH_3NH_3PbBr_3$ (235–150 K), but reappear abruptly at the transitions to the cubic or orthorhombic phases. The position of the $CH_3NH_3PbBr_3$ resonance peaks (Fig. 2) can be clearly seen to shift to lower frequencies with reducing temperature in the stability field of the cubic structure (∼300−235 K). The resonance peaks reappear and shift to higher frequencies in the stability field of the orthorhombic structure (< ∼150 K). From the present paper, the cubic-tetragonal transition is at 236 + / − 1 K, and the orthorhombic phase appears at ∼147 K during cooling.

Figure 4 shows the f^2 and Q^{-1} values of selected resonance peaks versus temperature for $CH_3NH_3PbBr_3$. Q^{-1} evolves in a similar way to $CH_3NH_3PbI_3$. Acoustic loss is low at the lowest temperatures in the orthorhombic region but starts to increase as the transition to tetragonal $CH_3NH_3PbBr_3$ is approached. Attenuation is extremely high in the tetragonal phase and diminishes sharply in the cubic phase. A significant difference between $CH_3NH_3PbI_3$ and $CH_3NH_3PbBr_3$ is how the frequency of the peaks changes in the orthorhombic region. In $CH_3NH_3PbBr_3$ stiffening occurs from 150 K down to 5 K without the reversal of this trend seen in $CH_3NH_3PbI_3$ below ∼100 K.

In view of the reports of an intermediate phase of $CH_3NH_3PbBr_3$, stable in a narrow temperature interval above the temperature at which the *Pnma* phase appears [32–35], spectra were collected in 1-K steps between 140 and 160 K. The variation of f^2 and Q^{-1} with temperature in this narrow interval is shown in Fig. 5. A sudden change in the trends of

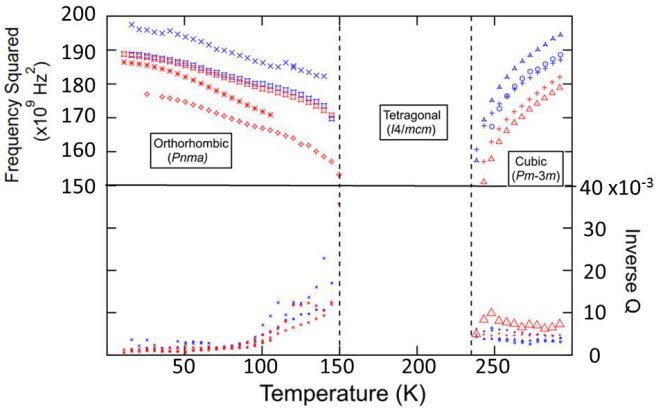

FIG. 4. f^2 and Q^{-1} values for resonance peaks in spectra collected from a single crystal of $CH_3NH_3PbBr_3$ during cooling (blue) and heating (red). Vertical dashed lines represent phase transitions. Due to high attenuation, it was not possible to follow resonance peaks in spectra collected between ∼150 and ∼235 K, corresponding to the expected limits for the stability field of the tetragonal phase. All f^2 values have been scaled so that they fit on the same plot.

f^2 and Q^{-1} above 148 K indicates a phase transition. There are also changes in the overall appearance of the spectra at 155 K and above, with several peaks disappearing and new peaks appearing at different frequencies. This is consistent with there being two transitions, at ∼147 and ∼154 K. The intermediate phase has elastic/anelastic characteristics which more closely resemble those of the tetragonal $I4/mcm$ phase than the orthorhombic *Pnma* phase. The transition at ∼147 K has a hysteresis of about 1 K, and the distribution of peaks from the intermediate phase is also different between heating and cooling. Differential scanning calorimetry (see Fig. S4 in the Supplemental Material [28]) confirms the presence of two transitions within this narrow temperature interval. The first transition occurs at 146 and 142 K (heating and cooling, respectively) and the second occurs at 151 and 148 K, giving average transition temperatures of 144 and 149 K, which are

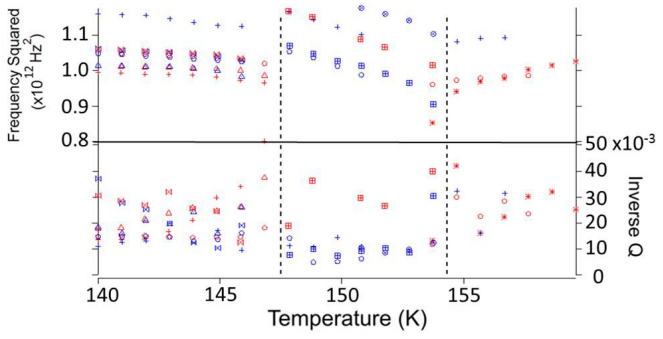

FIG. 5. Variation of f^2 and Q^{-1} with temperature for $CH_3NH_3PbBr_3$. Data were collected in a narrower temperature range using 1-K steps in the region around the expected orthorhombic-tetragonal phase transition. The dotted lines represent phase transitions. The peaks shown are in the 400–1200-kHz frequency range. Note that the Q^{-1} data display a relatively high degree of scatter because the resonance peaks become much more weakly defined at temperatures near to the phase transition.

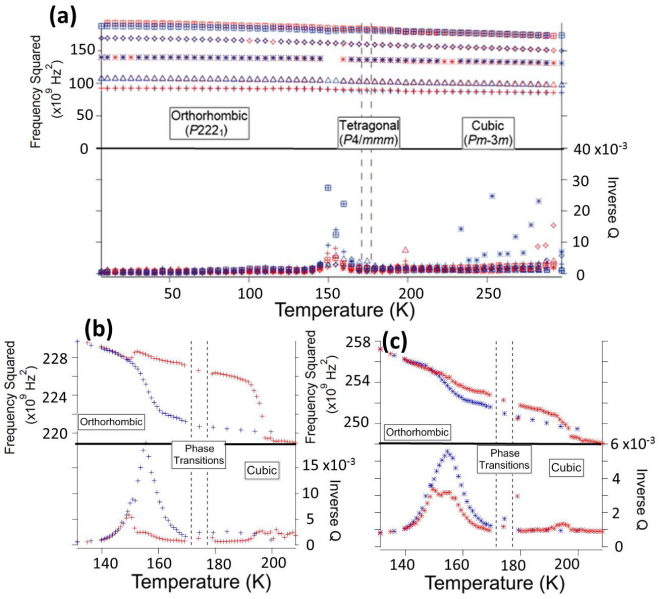

FIG. 6. Variation of f^2 and Q^{-1} with temperature for the resonance peaks in RUS spectra from a single crystal of $CH_3NH_3PbCl_3$. Dotted lines represent the expected phase transition temperatures. Blue points and red points represent values for the cooling sequence and the heating sequence, respectively. (a) Variation of f^2 and Q^{-1} values over the full temperature range. (b, c) Variation of f^2 and Q^{-1} values for 480 and 510 kHz, respectively, over a narrower temperature range. f^2 values in (a) are scaled so that all data points fit on the same plot. The symbols representing the peaks in (b) and (c) represent the same peaks in (a).

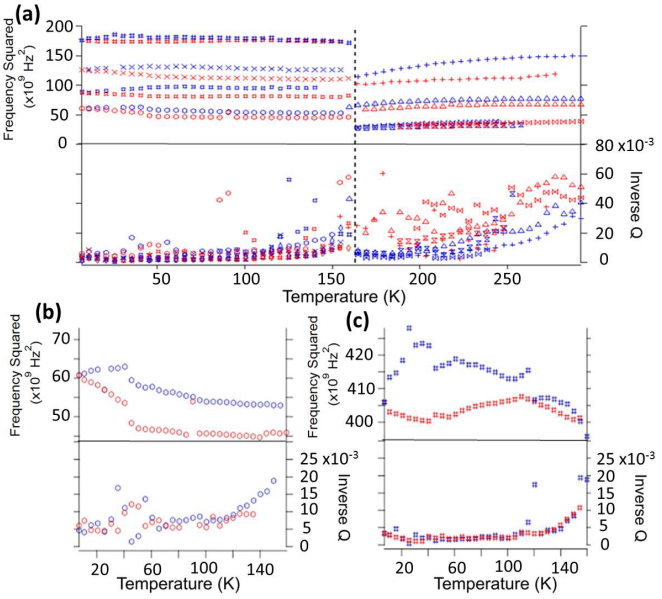

FIG. 7. Variation of f^2 and Q^{-1} with temperature over (a) the full temperature range and (b, c) a narrower temperature range, for selected resonance peaks in RUS spectra collected from a single crystal of $CD_3ND_3PbI_3$. (b) and (c) show the form of the anomalies in the evolution of f^2 for the selected resonance peaks and these may be indicative of an additional phase transition at ~40 K. The tetragonal-orthorhombic transition is marked with a vertical broken line. Data collected on cooling and heating are represented by blue and red points, respectively.

in reasonable agreement with the temperatures obtained from the RUS data. The DSC data also show a weak peak at 233 K, which can be attributed to the tetragonal-cubic transition.

C. Methylammonium lead chloride, $CH_3NH_3PbCl_3$

Primary RUS spectra collected for $CH_3NH_3PbCl_3$ in the temperature interval 5–295 K are shown in Fig. S5 in the Supplemental Material [28], and values of f^2 and Q^{-1} extracted for selected peaks are shown in Fig. 6(a). Overall, the resonance peaks barely shift in frequency across the entire temperature range, though there is an obvious increase in Q^{-1} centered at ~150 K. Hence $CH_3NH_3PbCl_3$ shows significantly different behavior from $CH_3NH_3PbBr_3$ and $CH_3NH_3PbI_3$ in that the known phase transitions at 171 and 177 K [36] appear to have only small and subtle effects on the elastic and anelastic properties. To examine the behavior at the transition points more closely, along with this anomalous spike in Q^{-1} values, spectra were collected during cooling and heating in 1-K steps between 140 and 210 K. The variations of f^2 and Q^{-1} with temperature for two of the most pronounced resonances, with frequencies near 480 and 510 kHz, are shown in Figs. 6(b) and 6(c).

1. Deuterated methylammonium lead iodide, $CD_3ND_3PbI_3$

In order to investigate the influence of hydrogen bonding in methylammonium lead iodide, RUS data were collected from a single crystal of deuterated $CH_3NH_3PbI_3$ ($CD_3ND_3PbI_3$). The variable temperature RUS spectra are shown in Fig. S6 in the Supplemental Material [28], and data for f^2 and Q^{-1} are given in Fig. 7. As can be seen from the spectra and from the data extracted from them (see Fig. S6 in the Supplemental Material [28] and Fig. 7), the temperature of the tetragonal to orthorhombic phase transition is barely changed by the exchange of deuterium for hydrogen. This in agreement with our results from DSC, shown in Fig. S7 in the Supplemental Material [28], which indicate transition temperatures of 161 and 155 K (heating and cooling, respectively) for the orthorhombic-tetragonal transition and 327 and 324 K for the cubic-tetragonal transition.

Like $CH_3NH_3PbI_3$ and $CH_3NH_3PbBr_3$, $CD_3ND_3PbI_3$ shows the same pattern of low Q^{-1} values (low acoustic loss) in the stability field of the orthorhombic structure. However, the introduction of deuterium into the system does cause some significant changes in behavior. First, there are many clear resonance peaks in spectra collected in the stability field of the tetragonal phase, showing that the acoustic attenuation is substantially lowered when D replaces H. Second, the elastic softening seen below ~110 K in the hydrogenated sample (Fig. 3) is not present in spectra from the deuterated sample (Fig. 7). Instead there is a break in the evolution of f^2 at a temperature of ~40 K, suggesting that there is an additional phase transition in the deuterated sample. Finally, there is a marked hysteresis for some resonances between cooling and heating such that the f^2 values during heating from ~5 K do not return to their values during cooling from 295 K. They remain different over the entire temperature range. Acoustic

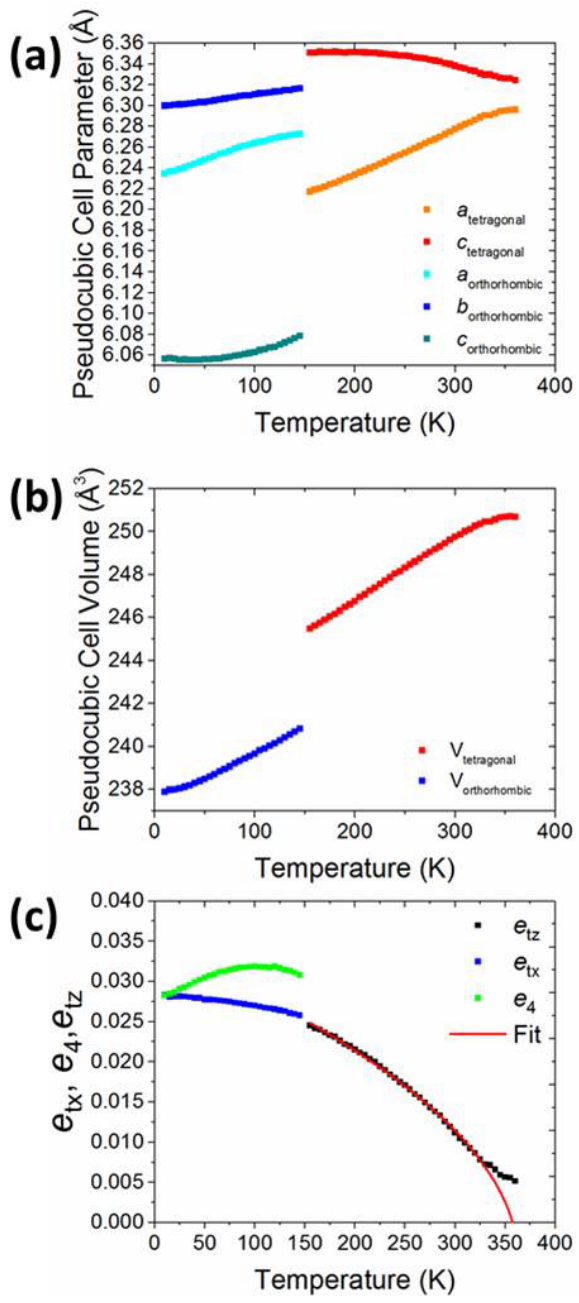

FIG. 8. Variation of (a) cell parameters and (b) cell volume with temperature for $CD_3ND_3PbI_3$ in the orthorhombic, tetragonal, and cubic regions. Due to the relatively fast ramp rate used and lack of equilibration time during the neutron-diffraction experiment, the sample did not fully convert to cubic $CD_3ND_3PbI_3$, hence only tetragonal cell parameters are shown in this temperature region. (c) Spontaneous strain obtained from lattice parameters over the full temperature range of the neutron-diffraction experiments. The curve through data for e_{tz} represents a fit for $e_{tz}^2 \propto (T_c - T)$. The tetragonal-orthorhombic transition is strongly first order.

loss in the stability field of the tetragonal phase is also higher during heating than during cooling.

The presence of resonance peaks in spectra from the tetragonal phase of the deuterated sample allows closer examination of the tetragonal-orthorhombic phase boundary. Rather irregular peaks, not corresponding to those of spectra from either of the tetragonal or orthorhombic phases in the interval between 158 and 163 K (during heating), imply that there may be a narrow two phase field consistent with the findings of Whitfield *et al.* [20] and the expected first-order character of the $I4/mcm$-$Pnma$ transition in perovskites. Interestingly this is in the same transition region where an anomaly occurs for the phase evolution of $CH_3NH_3PbBr_3$ as described above and reported as an incommensurate variant in [30]. Figure S7 in the Supplemental Material [28] shows part of the powder neutron-diffraction pattern collected on the same batch of samples between 150 and 160 K. A shoulder appears in the diffraction patterns at 155 K, corresponding to the tetragonal phase and showing that the tetragonal and orthorhombic phases coexist in a narrow temperature region, which is in agreement with reports in the literature [20].

Lattice parameters obtained from neutron diffraction are given in Fig. 8, and have been analyzed in terms of spontaneous strains [Fig. 8(c)] following the methodology described in detail by Carpenter *et al.* [37] and McKnight *et al.* [38]. A typical sequence of structural states which occurs in perovskites involves two tilt systems associated with R and M points of the reciprocal lattice of the parent cubic structure. The first tilt produces the $I4/mcm$ structure and the two tilt systems together produce the *Pnma* structure. Associated with these are three linear strains, e_1,e_2, and e_3, and one shear strain, e_4. Each of the strains couples with the square of the related order-parameter components, q_4 for the R point and q_2 for the M point. The objective here is to compare the magnitude and form of these strains for the case of methylammonium lead halides with the standard behavior of oxide perovskites. Expressions for determining values for the strain components $e_1 - e_4$ were taken from Table 2 of McKnight *et al.* and values of the reference parameter a_o of the cubic structure were estimated using $(a^2c/4)^{1/3}$ for the tetragonal structure and $(abc/4)^{1/3}$ for the orthorhombic structure. The resulting variations of symmetry adapted shear strains, $e_{tz} = (1/\sqrt{3})(2e_3 - e_1 - e_2)(\propto {q_4}^2)$, $e_{tx} = (1/\sqrt{3})(2e_1 - e_2 - e_3)$ $[\propto (Aq_2{}^2 - Bq_4{}^2)]$, and $e_4(\propto {q_4}^2)$, are shown in Fig. 8(c).

As an aside from the strain analysis, it is worth noting that there is a change in trend in the temperature dependence of e_4 below ~100 K [Fig. 8(c)]. In the orthorhombic structure, e_4 scales with ${q_4}^2$, where q_4 can be understood in terms of the M-point octahedral tilting of normal oxide perovskites [35]. The reduction in e_4 with falling temperature signifies that the tilting differs from $SrZrO_3$, for example, but it is not clear whether this is related to the break in elastic properties seen between ~40 and ~50 K in Fig. 7. Although there is a slight discontinuity in the b lattice parameter between ~40 and ~50 K, it is not significant enough to say with confidence that this is related to the break in elastic properties.

D. Comparing the photoluminescence of $CH_3NH_3PbI_3$ and $CD_3ND_3PbI_3$

To investigate the influence of phase transitions and hydrogen bonding on the performance of perovskite light emitting devices, the photoluminescence of both $CH_3NH_3PbI_3$ and $CD_3ND_3PbI_3$ was measured as a function of temperature down to 77 K. The variations of the peak wavelength and

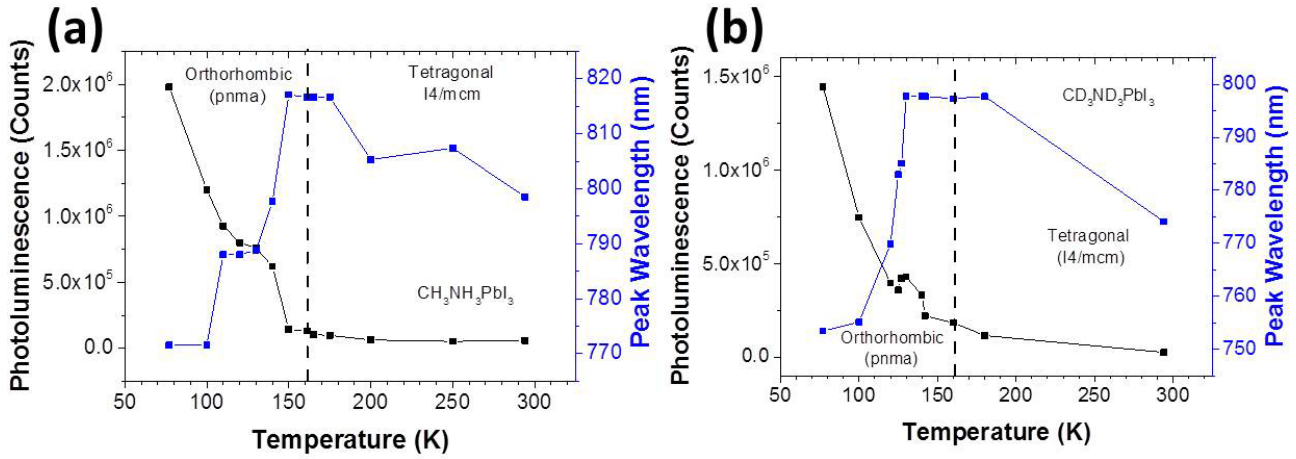

FIG. 9. Photoluminescence wavelength (blue data points) and intensity (black data points) vs temperature for (a) $CH_3NH_3PbI_3$ and (b) $CD_3ND_3PbI_3$. Dashed vertical lines represent the phase transition temperatures.

relative intensity with temperature are shown in Fig. 9, and the complete spectra are shown in Supplemental Material (Fig. S9) [28]. It is important to note that the PL was not measured using an integrating sphere, so it is valid to compare the PL counts on different measurements of the same sample, but the data cannot be used to compare absolute photoluminescence quantum yield between samples. It can be seen that the PL from $CD_3ND_3PbI_3$ is consistently blueshifted by approximately 20 nm compared to that from $CH_3NH_3PbI_3$. Both samples show a slow increase in peak wavelength with temperature up to approximately 180 K, where the peak wavelength remains constant across the phase transition. As they are cooled below a certain temperature (∼150 and ∼130 K for hydrogenated and deuterated samples, respectively) both samples exhibit a rapid blueshift of the photoluminescence, accompanied by a steep increase in the PL intensity with decreasing temperature. The increase in PL with decreasing temperature continues to the limit of our experimental range of 77 K, but the blueshift of the band gap appears to plateau for both samples at around 100 K.

IV. DISCUSSION

A. Octahedral tilting transitions

From the data for $CH_3NH_3PbBr_3$ (Fig. 4) and $CH_3NH_3PbI_3$ (Fig. 3) it is clear that the tetragonal ($I4/mcm$) phase has high acoustic loss, while the cubic and orthorhombic phases show very low loss. This closely mirrors the behavior of oxide perovskites such as (Ca,Sr)TiO_3 [39], which show the same sequence of octahedral tilting transitions. High loss in the tetragonal phase is attributed to the mobility under applied stress of the ferroelastic twin walls which arise when the first tilt system develops at the $Pm\bar{3}m$-$I4/mcm$ transition. These twins have recently been observed directly in $CH_3NH_3PbI_3$ by transmission electron microscopy [40]. For reasons that are not yet understood, the twin walls become immobile as soon as the second tilt system develops at the $I4/mcm$-$Pnma$ transition in oxide perovskites [14,39]. Softening in the cubic phase ahead of the cubic-tetragonal transition, as seen in Fig. 3 for $CH_3NH_3PbI_3$, is also typical of the oxide phases [38,39,41], and the elastic constants of the orthorhombic structure tend to be only weakly temperature dependent. The qualitative picture of both $CH_3NH_3PbBr_3$ and $CH_3NH_3PbI_3$ is therefore that they undergo classical octahedral tilting transitions and exhibit associated elastic/anelastic properties which are broadly similar to the same transitions in oxide perovskites.

Strain evolution at the cubic-tetragonal transition is also broadly similar in the halide and oxide systems. The tetragonal shear strain, e_{tz}, extracted from the neutron-diffraction data for $CD_3ND_3PbI_3$ shows that the transition is close to being tricritical in character [$e_{tz}^2 \propto q^4 \propto (T_c - T)$], as has been reported elsewhere for $CH_3NH_3PbI_3$ [20]. Essentially the same pattern of lattice parameter changes is seen also in $CH_3NH_3PbBr_3$ [42]. However the magnitude of the strain is much larger. The maximum values reached for the tetragonal strain in the $I4/mcm$ structure of (Ca,Sr)TiO_3 are ∼0.005 [43], whereas the maximum value for $CH_3NH_3PbI_3$ is ∼0.025 [Fig. 8(c)]. The perovskite structure consists of a three-dimensional network of corner sharing octahedra, so that macroscopic strains can be understood entirely in terms of tilting and distortion of the individual octahedra. Given that the maximum octahedral tilt angle, ϕ, is ∼9° in the halides [42,44] and ∼6° in the oxide example, and that the shear strain scales with ϕ^2, the large difference in strain between oxides and halides cannot be accounted for by just the difference in tilting angle—most must be due to the PbX_6 octahedra having larger or different distortions compared to TiO_6 octahedra.

Differences between the *Pnma* structures are more marked, in spite of the sequence of structure types being nominally the same. Values of the shear strains e_{tx} and e_4 for $CH_3NH_3PbI_3$ are each in the range ∼0.025−0.03 [Fig. 8(c)], but are much smaller in magnitude for (Ca,Sr)TiO_3 at ∼ −0.002 and ∼0.004, respectively [43]. The $I4/mcm$-$Pnma$ transition involves the same addition of a second octahedral tilt system in both cases but there must be other structural changes to account for the large difference in the lattice distortions which accompany it, and the origins of these most likely relate to hydrogen bonding.

B. Incipient instability in $CH_3NH_3PbI_3$

The elastic constants of most materials increase with falling temperature while the reverse, elastic softening, is

characteristic of the approach to a phase transition that might be proper ferroelastic, coelastic, or, as in the present case, improper ferroelastic. In this context, all the resonance modes of $CH_3NH_3PbI_3$ display softening by up to ~20% with falling temperature below ~100 K. There does not appear to be any discontinuity or abrupt change that would signify a discrete phase transition, however. Similar behavior to this has been observed in lanthanum aluminate ($LaAlO_3$) [45], though the magnitude of the softening observed here is nearly 20 times greater than in $LaAlO_3$. The interpretation for $LaAlO_3$ was of an incipient structural instability, and this is a possibility also for $CH_3NH_3PbI_3$. Given that the presence of the $(CH_3NH_3)^+$ cation adds other variables, instabilities due to hydrogen bonding or orientation of the $(CH_3NH_3)^+$ ions could also be responsible. The likely role of hydrogen bonding is emphasized by the contrasting behavior of $CD_3ND_3PbI_3$ which has a relatively sharp change (stiffening) in elastic properties at ~40 K in place of the continuous softening. Further investigation will be needed to determine the underlying structural mechanism(s) definitively.

C. Effects of hydrogen bonding

One of the key features of methylammonium lead halide perovskites which make them different from their oxide counterparts is the organic cation. Therefore hydrogen bonding and the orientation of the cation are additional structural variables that can contribute to the structure-property relationships. Several experimental and theoretical studies have looked at the importance of hydrogen bonding in $CH_3NH_3PbI_3$. Neutron-diffraction studies on deuterated samples have shown that the hydrogen/deuterium atoms bonded to nitrogen in the methylammonium cation form the strongest hydrogen bonds with the iodine atoms [20]. This is indicated by short H/D-I distances in $CH_3NH_3PbI_3$, and by the fact that its cubic phase exhibits weaker hydrogen bonding than the other polymorphs. Separating the influence of octahedral tilting from the hydrogen bonding is not trivial, although several studies have tried to determine whether the octahedral tilting drives the hydrogen bonding or *vice versa* [46–49]. Lee *et al.* have found that the hydrogen bonding helps stabilize octahedral tilts, and have suggested that tuning the directionality of hydrogen bonding may also influence the photophysical properties [46].

The influence of the hydrogen bonding could also provide an explanation for why the halide perovskites have such unusually high lattice strains compared to their oxide counterparts. Swainson *et al.* [50] have shown that the orientation of the $CH_3NH_3^+$ cation is strongly disordered in the cubic and tetragonal structures, but it becomes ordered in the *Pnma* structure so as to optimize hydrogen bonding. $CH_3NH_3PbBr_3$, $CH_3NH_3PbI_3$, and $CD_3ND_3PbI_3$ all adopt a *Pnma* structure which allows optimization of hydrogen bonding with the perovskite framework, and this provides a possible explanation for the high shear strains.

Hydrogen bonding plays an even larger role in $CH_3NH_3PbCl_3$ because the radius ratio criteria for tilting transitions are no longer met, and so the structural phase transitions near 175 K appear to be driven predominantly by hydrogen bonding [51], arising from an ordering in the configuration of the methylammonium groups on the lattice A sites. The sequence with falling temperature is again cubic-tetragonal-orthorhombic, but the intermediate structure of $CH_3NH_3PbCl_3$ may be incommensurate [51]. Although the space group of the orthorhombic structure is again *Pnma*, the unit cell ($2a\times2a\times2a$, where a represents the cell edge of the parent cubic structure) is different from that of the tilted structure ($\sqrt{a}\times\ 2a\times\sqrt{a}$).

While it is relatively straightforward to understand the influence of hydrogen bonding on structural evolution with temperature, there appears also to be a more subtle effect on twin wall dynamics. Acoustic loss in the stability field of the tetragonal phase of $CD_3ND_3PbI_3$ is significantly less than for the same phase of $CH_3NH_3PbI_3$ (compare Figs. 3 and 7). This acoustic loss is an indication of the effective viscosity experienced by a twin wall as it moves through the crystal under the influence of an external stress. As discussed for the case of twin wall loss mechanisms in $LaAlO_3$ [45], the viscosity may be extrinsic, due to the interaction of the twin walls with defects, or it may be intrinsic, such as by interaction with phonons. Both mechanisms could apply in the present case but the important point is that the exchange of H for D provides a previously unrecognized means of controlling the dynamics of twin wall motion, in the wider context of "domain wall engineering" for new device applications [52,53].

Changes of the configuration of pinned twin walls can also explain the hysteresis observed in the frequencies of some of the resonances in spectra from the tetragonal and orthorhombic phases of $CD_3ND_3PbI_3$ (see Fig. 7). If all possible transformation twins are present in equal proportions, the effective macroscopic symmetry of the crystal will be cubic. However, if there is a preponderance of one twin orientation, the macroscopic symmetry will be broken and the effective elastic constants will depend on their precise configuration. On this basis it appears that a change in twin configuration occurs on cooling to the lowest temperatures but is not reversed exactly on heating.

Comparing the data for $CH_3NH_3PbI_3$ in Fig. 3 with the data for $CD_3ND_3PbI_3$ in Fig. 7 shows that acoustic loss is significantly lower in the deuterated sample and this has been discussed in terms of differences in the effective viscosity experienced by mobile twin walls even before the ordering of H/D bonds becomes established. It is also clear from the lack of elastic stiffening in $CD_3ND_3PbI_3$ that, although strain coupling with the order parameter is strong in all cases, the dynamics of relaxations in tilting are quite different (i.e., fast) from hydrogen bonding (slow) under the influence of external stress.

D. Chloride versus bromide and iodide

The acoustic properties of $CH_3NH_3PbBr_3$ and $CH_3NH_3PbI_3$ are broadly similar to those of oxide perovskites and can be understood in terms of classical strain coupling to the order-parameter. A stress is applied which induces a strain which, in turn, induces a relaxation of the order parameter so that the crystal is elastically softer than it would have been if there was no such coupling. In general, the magnitude of the softening is related to the strength of the coupling, as measured by the magnitudes of the spontaneous strains [54,55]. Individual linear strains of the

Pnma structure of $CH_3NH_3PbCl_3$, with respect to the parent cubic structure, are at the 1% level [51] and large anomalies would also be expected to occur. However, the resonance peaks in $CH_3NH_3PbCl_3$ barely change position over the full temperature range, and the two known phase transitions at 171 and 177 K have no overt impact on the acoustic loss (represented by Q^{-1}) or the elastic constants (represented by f^2). The implication is that application of a stress in an RUS experiment at ∼1 MHz does not induce a relaxation of the order parameter. In other words, the configuration of hydrogen bonds responsible for the lattice distortions remains fixed, at least on a time scale of $\sim 10^{-6}$ s. In the mineral lawsonite, $CaAl_2Si_2O_7(OH)_2 \cdot H_2O$, development of hydrogen bonding also drives phase transitions which are not accompanied by any elastic softening [26,56,57]. Instead, substantial stiffening occurs and the pattern of ordered hydrogen bonds is understood to provide effective braces through the crystal. For the perovskite structure it appears that the additional hydrogen bonding does not have the same bracing effect, presumably because the bonds are relatively weak in comparison with the framework of metal-halide bonds already present.

There are significant anelastic effects evident in the RUS data for $CH_3NH_3PbCl_3$, however, and these show that the cubic-orthorhombic transition occurs in two dynamical parts when examined at RUS frequencies. The association of a peak in Q^{-1} with slight stiffening with falling temperature is typical of a Debye resonance effect associated with some freezing process that is coupled with strain [58]. The loss peak is observed when the relaxation time (τ) of the relaxation overlaps with one of the acoustic resonances of the sample such that $\omega\tau = 1$, where $\omega(=2\pi f)$ is the angular frequency of the resonance with frequency f. The activation energy for a thermally activated process is typically determined by measuring loss under conditions of variable frequency at constant temperature. In an RUS experiment, the measurement is done effectively as a function of temperature at more or less constant frequency. This has been successfully analyzed in a number of cases [14] using the function

$$Q^{-1}(T) = Q_{\mathrm{m}}^{-1}\left[\cosh\left\{\frac{E_{\mathrm{a}}}{Rr_2(\beta)}\left(\frac{1}{T}-\frac{1}{T_{\mathrm{m}}}\right)\right\}\right]^{-1} \quad (1)$$

where the maximum value of Q^{-1}, Q_m^{-1}, occurs at temperature T_{m} and the temperature dependence is determined by the activation energy, E_{a}, combined with a spread of relaxation times described by the term $r_2(\beta)$ [59,60]. R is the gas constant and $r_2(\beta) = 1$ if there is only one relaxation time.

Fitting Eq. (1) to the single loss peak at ∼155 K in the cooling cycle gave activation energies ranging between 340 and 600 meV. The presence of multiple peaks around 155 K in the heating cycle suggests that several distinct relaxation processes occur during heating and cooling through the transition temperature interval, and fits to these give values of E_{a} in the range 350–840 meV (Fig. 10). We suggest that the lower E_{a} processes represent a freezing in the rotation of the $CH_3NH_3^+$ cation, while the higher-energy processes represent the motion of the Cl^- ions between lattice vacancies. The latter is a known effect in this class of perovskites, and has recently attracted considerable interest because of its detrimental effect on the band-gap tuneability of these materials [61]. This halide migration was found to have an activation energy of 0.6 eV by Eames *et al.* [62], which agrees closely with the activation energy we observe here. There are less available data on the freezing of the $CH_3NH_3^+$ cation, but Chen *et al.* [63] recently reported that the $CH_3NH_3^+$ cation in $CH_3NH_3PbI_3$ has a rotational degree of freedom with an activation energy of approximately 80 meV, which differs significantly from our result. This could be due to the slightly different, nontilted structure of $CH_3NH_3PbCl_3$ compared to $CH_3NH_3PbI_3$, and future work could focus on how this freezing effect changes when the $CH_3NH_3^+$ cation is replaced with $CD_3ND_3^+$, $CH(NH_2)(NH_3)^+$, or Cs^+ ions so as to confirm that the A site cation is the cause of this freezing. Also shown in Fig. 10 are fits to some of the smaller peaks which appear at ∼195 K, giving values of E_{a} of 1.7–2.2 eV, which we suggest corresponds to movement of the Pb^{2+} ion, which was calculated by Eames *et al.* to have an activation energy of 2.3 eV [62].

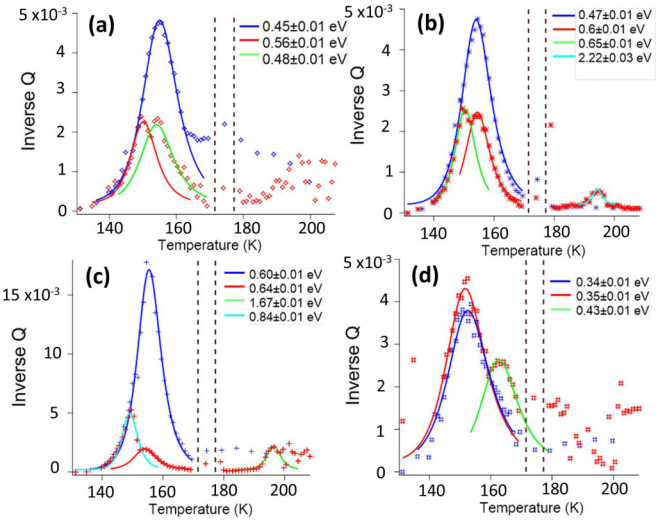

FIG. 10. Fits of Eq. (1) to selected loss peaks at (a) 1020 kHz, (b) 510 kHz, (c) 480 kHz, and (d) 290 kHz, respectively, for resonances observed during cooling (blue) and heating (red). A constant baseline is removed from each data set prior to fitting. The values of E_a shown for each peak are under the assumption that $r_2(\beta) = 1$. Activation energies for each fit are shown in the legend.

From the perspective of strain and elasticity, the phase transitions in $CH_3NH_3PbCl_3$ seem to be split into different components, relating to orientational disorder of the A site cation and its interaction with the perovskite framework by hydrogen bonding. These effects have a marked hysteresis between cooling and heating when measured at frequencies in the vicinity of 1 MHz.

E. Relevance to orientational glass phases

The impact which the freezing of the $CH_3NH_3^+$ cation has on the structure-property relations of hybrid perovskites is a subject of great interest, and previous studies on perovskites have gained insight into this by drawing comparisons with alkali-metal cyanides such as NaCN or KCN. In these cases the strongly preferred orientation of the CN^- ion leads to the formation of "orientational glass" phases [64]. In hybrid perovskites, the $CH_3NH_3^+$ cation has been reported to have

no preferred orientation when in the cubic and tetragonal phases. But in $CH_3NH_3PbI_3$ and $CH_3NH_3PbBr_3$ the tetragonal to orthorhombic phase transition is associated with a partial freezing because the A site becomes too distorted to allow free rotation and the rotation is limited to be along the C-N axis with a slow freezing of this motion on the approach to absolute zero [65]. In agreement with this, we see no evidence of sudden freezing of MA cations in $CH_3NH_3PbI_3$ and $CH_3NH_3PbBr_3$ RUS spectra, but Fabini *et al.* [65] recently reported that the substitution of $CH_3NH_3^+$ with formamidinium ions introduces a geometric frustration to the hydrogen bonding which significantly alters the phase evolution of the material and causes the A site cations to undergo glassy freezing below 50 K. This further underscores how hydrogen bonding can drive the structural evolution.

Mozur *et al.* [66] also recently reported that partially substituting $CH_3NH_3^+$ with Cs ions can also cause the remaining $CH_3NH_3^+$ cations to form an orientational glass due to the changing geometry of octahedra. Doping will have this effect because it must lead to changes in coordination and local distortions which would limit ion rotation and mobility. From our own data, $MAPbCl_3$ does not have tilting transitions, and so the rotation of the cations is not suddenly limited by the change in site geometry. Hence we are able to observe the freezing happening directly (via Debye resonance) rather than having it hidden within a phase transition.

F. Implications for photoluminescence properties

As discussed earlier, it is of great interest to determine how the different processes analyzed in this paper impact the light emitting properties of methylammonium lead halides. From Fig. 9, we see that the PL does not change across the tetragonal to orthorhombic phase transition, indicating that the phase of the perovskite has little direct impact on the behavior of the PL. However, in the case of $CH_3NH_3PbI_3$, there appears to be a much more significant process occurring at 150 K which causes the PL to abruptly blueshift and increase significantly in intensity. It is likely that this effect is strongly related to hydrogen bonding within the crystal because the $CD_3ND_3PbI_3$ sample exhibits the same behavior but at a slightly lower temperature. This difference can only be due to the exchange of D for H with the heavier $CD_3ND_3^+$ cation causing the process to occur at a lower temperature, but further study is needed to confirm the exact origin of this effect.

Direct strain effects appear to be less important. The relatively large spontaneous strains associated with tilting appear to not make any real difference to the PL properties. On the other hand, hydrogen bonding can stabilize orthorhombic structures irrespective of whether tilting occurs. Therefore, the imposition of a large strain on a thin film by choice of appropriate substrate might significantly change the dynamics of the A site cation, and hence allow modulation of the PL properties. As of yet there is no sign that twin walls, whether mobile or immobile, have any bearing on the PL characteristics. In a different context, it is certainly of interest from the wider perspective of domain-wall engineering that the presence of an organic A cation with choice of H or D could be used to control the effective viscosity experienced by a moving twin wall.

V. CONCLUSIONS

In conclusion, this paper presents a study of the material properties of methylammonium lead halides using a combination of resonant ultrasound spectroscopy, neutron powder diffraction, differential scanning calorimetry, and photoluminescence. We find that $CH_3NH_3PbI_3$ and $CH_3NH_3PbBr_3$ undergo tilting transitions analogous to $(Ca,Sr)TiO_3$, with the exception that the lattice strain is close to an order of magnitude greater than those usually observed in oxide perovskites. $CH_3NH_3PbI_3$ also displays a softening behavior below $\sim$100 K which suggests that there is an additional incipient structural instability in the crystal. $CH_3NH_3PbCl_3$ does not undergo tilting transitions, and this has allowed us to observe a band of anelastic behavior at $\sim$150 K which allowed us to calculate the activation energy of several freezing processes within the crystal. We finally show that deuterating the $CH_3NH_3PbI_3$ structure has a significant impact on the behavior of the photoluminescence with temperature, on the movement of the twin walls in the tetragonal phase, and on the incipient instability observed at low temperature. This would suggest that all of these processes are governed to some degree by the hydrogen bonding in the methylammonium cation. For research data underpinning this paper, see [67].

ACKNOWLEDGMENTS

This paper was supported by Engineering and Physical Sciences Research Council (EPSRC) Grants No. EP/K503162/1, No. EP/M506631/1, No. EP/M025330/1, No. EP/L017008/1, No. EP/K022237/1, No. EP/K015540/1, and No. EP/I036079/1. RUS facilities in Cambridge were established through grants to M.A.C. from the EPSRC and the Natural Environment Research Council (Grants No. NE/B505738/1 and No. NE/F17081/1). A portion of this research used resources at the Spallation Neutron Source, a U.S. Department of Energy Office of Science User Facility operated by the Oak Ridge National Laboratory (ORNL). I.D.W.S. acknowledges funding from a Royal Society Wolfson research merit award. Finally, we would like to thank George M. Carins and Dr. Dragos Neagu (University of St Andrews) and Dr. Melanie Kirkham (ORNL) for support during the neutron-diffraction experiments.

[1] A. Kojima, K. Teshima, Y. Shirai, and T. Miyasaka, J. Am. Chem. Soc. **131**, 6050 (2009).
[2] N. G. Park, Mater. Today **18**, 65 (2015).
[3] N. N. Wang *et al.*, Nat. Photon. **10**, 699 (2016).
[4] G. L. Whitworth, J. R. Harwell, D. N. Miller, G. J. Hedley, W. Zhang, H. J. Snaith, G. A. Turnbull, and I. D. W. Samuel, Optics Express **24**, 23677 (2016).
[5] Y. P. He and G. Galli, Chem. Mater. **26**, 5394 (2014).

[6] A. R. S. Kandada and A. Petrozza, Accounts Chem. Res. **49**, 536 (2016).

[7] S. D. Stranks, G. E. Eperon, G. Grancini, C. Menelaou, M. J. P. Alcocer, T. Leijtens, L. M. Herz, A. Petrozza, and H. J. Snaith, Science **342**, 341 (2013).

[8] K. Chen, A. J. Barker, F. L. C. Morgan, J. E. Halpert, and J. M. Hodgkiss, J. Phys. Chem. Lett. **6**, 153 (2015).

[9] J. R. Harwell, T. K. Baikie, I. D. Baikie, J. L. Payne, C. Ni, J. T. S. Irvine, G. A. Turnbull, and I. D. W. Samuel, Phys. Chem. Chem. Phys. **18**, 19738 (2016).

[10] F. Hao, C. C. Stoumpos, P. J. Guo, N. J. Zhou, T. J. Marks, R. P. H. Chang, and M. G. Kanatzidis, J. Am. Chem. Soc. **137**, 11445 (2015).

[11] C. Motta, F. El-Mellouhi, and S. Sanvito, Sci. Rep. **5**, 12746 (2015).

[12] A. Pisoni, J. Jacimovic, O. S. Barisic, M. Spina, R. Gaal, L. Forro, and E. Horvath, J. Phys. Chem. Lett. **5**, 2488 (2014).

[13] G. Grancini, V. D'Innocenzo, E. R. Dohner, N. Martino, A. R. Srimath Kandada, E. Mosconi, F. De Angelis, H. I. Karunadasa, E. T. Hoke, and A. Petrozza, Chem. Sci. **6**, 7305 (2015).

[14] M. A. Carpenter, J. Phys.: Condens. Matter **27**, 263201 (2015).

[15] B. J. Zadler, J. H. L. Le Rousseau, J. A. Scales, and M. L. Smith, Geophys. J. Int. **156**, 154 (2004).

[16] L. G. Tang and W. W. Cao, J. Vis. Exp. **110**, 53461 (2016).

[17] A. Shekhter, B. J. Ramshaw, R. Liang, W. N. Hardy, D. A. Bonn, F. F. Balakirev, R. D. McDonald, J. B. Betts, S. C. Riggs, and A. Migliori, Nature (London) **498**, 75 (2013).

[18] O. Svitelskiy, A. V. Suslov, J. B. Betts, A. Migliori, G. Yong, and L. A. Boatner, Phys. Rev. B **78**, 064113 (2008).

[19] W. Travis, E. N. K. Glover, H. Bronstein, D. O. Scanlon, and R. G. Palgrave, Chem. Sci. **7**, 4548 (2016).

[20] P. S. Whitfield, N. Herron, W. E. Guise, K. Page, Y. Q. Cheng, I. Milas, and M. K. Crawford, Sci. Rep. **6**, 35685 (2016).

[21] M. T. Weller, O. J. Weber, P. F. Henry, A. M. Di Pumpo, and T. C. Hansen, Chem. Commun. **51**, 4180 (2015).

[22] W. D. Xu, L. J. Liu, L. J. Yang, P. F. Shen, B. Q. Sun, and J. A. McLeod, Nano Lett. **16**, 4720 (2016).

[23] A. M. A. Leguy *et al.*, Nat. Commun. **6**, 7124 (2015).

[24] A. C. Larson and R. B. Von Dreele, General Structure Analysis System (GSAS), Los Alamos National Laboratory Report LAUR 86-748 (2004).

[25] B. H. Toby, J. Appl. Crystallogr. **34**, 210 (2001).

[26] R. E. A. McKnight, M. A. Carpenter, T. W. Darling, A. Buckley, and P. A. Taylor, Am. Mineral. **92**, 1665 (2007).

[27] R. E. A. McKnight, T. Moxon, A. Buckley, P. A. Taylor, T. W. Darling, and M. A. Carpenter, J. Phys.: Condens. Matter **20**, 075229 (2008).

[28] See Supplemental Material at http://link.aps.org/supplemental/10.1103/PhysRevMaterials.2.065404 for the complete RUS spectra for all samples, along with raw spectra from DSC and PL measurements.

[29] T. Baikie, Y. N. Fang, J. M. Kadro, M. Schreyer, F. X. Wei, S. G. Mhaisalkar, M. Graetzel, and T. J. White, J. Mater. Chem. A **1**, 5628 (2013).

[30] C. C. Stoumpos, C. D. Malliakas, and M. G. Kanatzidis, Inorg. Chem. **52**, 9019 (2013).

[31] M. S. Alvar, M. Kumar, P. W. M. Blom, G. J. A. H. Wetzelaer, and K. Asadi, AIP Adv. **7**, 095110 (2017).

[32] A. Poglitsch and D. Weber, J. Chem. Phys. **87**, 6373 (1987).

[33] I. P. Swainson, C. Stock, S. F. Parker, L. Van Eijck, M. Russina, and J. W. Taylor, Phys. Rev. B **92**, 100303(R) (2015).

[34] O. Knop, R. E. Wasylishen, M. A. White, T. S. Cameron, and M. J. M. Vanoort, Can. J. Chem. **68**, 412 (1990).

[35] N. Onodayamamuro, O. Yamamuro, T. Matsuo, and H. Suga, J. Phys. Chem. Solids **53**, 277 (1992).

[36] N. Onodayamamuro, T. Matsuo, and H. Suga, J. Phys. Chem. Solids **51**, 1383 (1990).

[37] M. A. Carpenter, A. I. Becerro, and F. Seifert, Am. Mineral. **86**, 348 (2001).

[38] R. E. A. McKnight, C. J. Howard, and M. A. Carpenter, J. Phys.: Condens. Matter **21**, 015901 (2009).

[39] N. J. Perks, Z. Zhang, R. J. Harrison, and M. A. Carpenter, J. Phys.: Condens. Matter **26**, 505402 (2014).

[40] M. U. Rothmann, W. Li, Y. Zhu, U. Bach, L. Spiccia, J. Etheridge, and Y. B. Cheng, Nat. Commun. **8**, 14547 (2017).

[41] R. E. A. McKnight, B. J. Kennedy, Q. Zhou, and M. A. Carpenter, J. Phys.: Condens. Matter **21**, 015902 (2009).

[42] H. Mashiyama, Y. Kawamura, E. Magome, and Y. Kubota, J. Korean Phys. Soc. **42**, S1026 (2003).

[43] M. A. Carpenter, C. J. Howard, K. S. Knight, and Z. Zhang, J. Phys.: Condens. Matter **18**, 10725 (2006).

[44] Y. Kawamura, H. Mashiyama, and K. Hasebe, J. Phys. Soc. Jpn. **71**, 1694 (2002).

[45] M. A. Carpenter, A. Buckley, P. A. Taylor, R. E. A. McKnight, and T. W. Darling, J. Phys.: Condens. Matter **22**, 035405 (2010).

[46] J. H. Lee, N. C. Bristowe, S. H. Lee, P. D. Bristowe, A. K. Cheetham, and H. M. Jang, Chem. Mater. **28**, 4259 (2016).

[47] J. R. Li and P. Rinke, Phys. Rev. B **94**, 045201 (2016).

[48] J. H. Lee, N. C. Bristowe, P. D. Bristowe, and A. K. Cheetham, Chem. Commun. **51**, 6434 (2015).

[49] J. H. Lee, E. H. Kong, and H. M. Jang, Sci. Rep. **6**, 21687 (2016).

[50] I. P. Swainson, R. P. Hammond, C. Soulliere, O. Knop, and W. Massa, J. Solid State Chem. **176**, 97 (2003).

[51] L. S. Chi, I. Swainson, L. Cranswick, J. H. Her, P. Stephens, and O. Knop, J. Solid State Chem. **178**, 1376 (2005).

[52] E. Salje and H. L. Zhang, Phase Transit. **82**, 452 (2009).

[53] E. K. H. Salje, Chemphyschem **11**, 940 (2010).

[54] W. Rehwald, Adv. Phys. **22**, 721 (1973).

[55] M. A. Carpenter and E. K. H. Salje, Eur. J. Mineral. **10**, 693 (1998).

[56] P. Sondergeld, W. Schranz, A. Troster, T. Armbruster, G. Giester, A. Kityk, and M. A. Carpenter, Am. Mineral. **90**, 448 (2005).

[57] M. A. Carpenter, Am. Mineral. **91**, 229 (2006).

[58] B. Norwick, *Anelastic Relaxation in Crystalline Solids* (Academic Press, New York, 1972).

[59] M. Weller, G. Y. Li, J. X. Zhang, T. S. Ke, and J. Diehl, Acta Metall. Mater. **29**, 1047 (1981).

[60] R. Schaller, *Mechanical Spectroscopy Q-1 2001: With Applications to Materials Science* (Trans Tech, Switzerland, 2001).

[61] W. Rehman, D. P. McMeekin, J. B. Patel, R. L. Milot, M. B. Johnston, H. J. Snaith, and L. M. Herz, Energ. Environ. Sci. **10**, 361 (2017).

[62] C. Eames, J. M. Frost, P. R. F. Barnes, B. C. O'Regan, A. Walsh, and M. S. Islam, Nat. Commun. **6**, 7497 (2015).

[63] T. Chen, B. J. Foley, B. Ipek, M. Tyagi, J. R. D. Copley, C. M. Brown, J. J. Choi, and S. H. Lee, Phys. Chem. Chem. Phys. **17**, 31278 (2015).

[64] J. Even, M. Carignano, and C. Katan, Nanoscale **8**, 6222 (2016).

[65] D. H. Fabini, T. A. Siaw, C. C. Stoumpos, G. Laurita, D. Olds, K. Page, J. G. Hu, M. G. Kanatzidis, S. Han, and R. Seshadri, J. Am. Chem. Soc. **139**, 16875 (2017).

[66] E. M. Mozur, A. E. Maughan, Y. Q. Cheng, A. Hug, N. Jalarvo, L. L. Daemen, and J. R. Neilson, Chem. Mater. **29**, 10168 (2017).

[67] The research data underpinning this paper can be accessed at http://dx.doi.org/10.17630/4f06e816-a2db-4665-ac43-8e1b475f6e6c.